



Remotely Sensed and Empirical Reference Evapotranspiration Models to Derive Crop Coefficients for Pistachios in the Central Basin of Iran

Fatemeh Firoozi¹ · Seyed Kazem Alavipanah² · Seyed Zeynalabedin Hosseini³ · Shamsollah Asgari⁴ · Hamid Reza Ghafarian Malamiri⁵ · Kamran Rahimi⁶

Received: 13 November 2021 / Accepted: 3 June 2023 / Published online: 22 July 2023
© The Author(s), under exclusive licence to Shiraz University 2023

Abstract

The main objective of this study is to estimate the actual evapotranspiration rate and determine the water requirement of pistachio crops in the central plateau of Iran using satellite remote sensing products. In order to achieve this main goal, 12 images from the Operational Earth Imager (OLI) of the Landsat 8 satellite for the water year 2018–2019 were downloaded from NASA's Land Processes Distributed Active Archive Center. The daily data of the five variables, namely maximum temperature, minimum temperature, wind speed, relative humidity, and sunshine hours of Taft station, were also obtained from the Iran Meteorological Organization as the closest meteorological station to the study area after preparing images and collecting data. First, the actual evapotranspiration rate of the pistachio product was estimated on a monthly scale for every 12 months of the study using two surface energy balance (SEBAL) and Surface Energy Balance Index (SEBS). Evapotranspiration potential was also acquired in a station scale applying 12 experimental methods. In a comparative study, the results revealed that the evapotranspiration values achieved from the four experimental models H–S, B–C, Trabert, and Rn-Based, have the highest correlation and the lowest error value with the values estimated from the two SEBAL and SEBS models. Finally, the water requirement of the pistachio crop during its growth period was estimated separately using two models, namely SEBAL and SEBS, and confirmed the experimental models.

Keywords Arid area · Evapotranspiration · SEBAL · SEBS · Water requirement · Experimental models

1 Introduction

Vegetation growth is constantly affected by different environmental factors. Therefore, environmental stresses are the most important factors reducing the yield of

agricultural products in the world (Franklin et al. 2010). Environmental stresses generally decrease crop yields by about 71%, among which the effect of high temperature of 15% and low temperature of 14%, water stress of 17%, and salinity stress of 20% have been estimated as yield loss

✉ Seyed Zeynalabedin Hosseini
zhosseini@yazd.ac.ir

Fatemeh Firoozi
firozif@yahoo.com

Seyed Kazem Alavipanah
salavipa@ut.ac.ir

Shamsollah Asgari
s.hamsasgari@yahoo.com

Hamid Reza Ghafarian Malamiri
h.rghafarian@gmail.com

Kamran Rahimi
kamranrahimi30@yahoo.com

² Department of Remote Sensing and GIS, Faculty of Geography, University of Tehran, Tehran, Iran

³ Faculty of Natural Resources and Desert Studies, Yazd University, Yazd, Iran

⁴ Soil Conservation and Watershed Management Research Department, Ilam Agricultural and Natural Resources Research and Education Center, Agricultural Research, Education and Extension Organization (AREEO), Tehran, Iran

⁵ Department of Geography, Yazd University, Yazd, Iran

⁶ Master of Remote Sensing, Kharazmi University, Tehran, Iran

¹ Department of Remote Sensing and Geographical Information System (GIS), Faculty of Geography, University of Tehran, Tehran, Iran

factors (Ranjbar and Anosheh 2015). Drought, on the other hand, is one of the limiting and threatening factors for successful production of crops (Spaeth et al. 1984). The rate of yield reduction due to moisture stress depends on the genotype, plant development stage, severity, and duration of water shortage, but the negative effects of these stresses are greater during flowering, seed formation, and fill ratio (Spaethetal 1984). Plants cope with water stress by reducing growth parameters, pores closure, and reducing photosynthesis (Fabriki Ourang and Mehrabad 2018) and these factors also affect the rate of plant evapotranspiration.

Evapotranspiration, which also includes evaporation of water from the soil and the transpiration of vegetation, represents a fundamental trend in hydrological cycles and a key element of water resources management, especially in arid and semi-arid regions (Gao et al. 2008).

As mentioned, evapotranspiration is one of the important factors in the hydrological cycle (Shamloo et al. 2021) and one of the determining factors of the energy equation at the surface of the earth and its estimation is needed in various fields, such as hydrology, agriculture, forest and rangeland management, and water resource management (Miryaghoubzadeh 2014). Generally, 64% of precipitation is out of reach due to evapotranspiration. In fact, evapotranspiration is the major link between the elements of the earth and the atmosphere (Su et al. 2006). Variables such as radiation, temperature, humidity, wind, and soil moisture, are the variables that affect the rate of evapotranspiration. Therefore, the amount of wasted water by evapotranspiration is more than the runoff in agricultural lands (Sumner 2001).

In fact, evapotranspiration is the most important element of the air and climate after temperature and rainfall. Evapotranspiration plays an important role in heat and mass drifts of the global atmospheric system and plays a key role in international scientific programs (Ehlers and Krafft 1996).

Due to changes in land use, land cover, physical characteristics of soil, and surface currents, hydrological and meteorological parameters show major changes that can be estimated with a limited number of synoptic observations (Bastiaanssen et al. 1997). Evapotranspiration is very important in water and agricultural resources management. There are many factors involved in evapotranspiration, so estimating evapotranspiration is a very difficult task. During the last half century, numerous experimental methods have been proposed by researchers globally to estimate potential evapotranspiration. These methods are classified into five groups: combined, temperature, radiation, humidity, and evaporation pan (Sharifan et al. 2006).

Some researchers suggest the use of traditional methods that require less meteorological parameters such as Irmak, Tabari, Trajkovic, Bereti, Blaney Cridle, Rozani et al.,

Rn-Based, and Droogers Allen (Tabari et al. 2011). However, these methods determine the rate of evapotranspiration at a small area for specific times and cannot be used for larger areas. Therefore, evapotranspiration estimation models can be used to overcome this limitation (Matin and Bourque 2013; Dinesh et al. 2014; Bastiaanssen et al. 1998; Rahimizadegan and Jahani 2019).

Satellite images can be used to determine ET over wide areas in these models. In a more comprehensive statement, satellite remote sensing models provide relatively accurate estimates of ET over large areas with minimal use of terrestrial data and multiple algorithms (Bastiaanssen and Chandrapala 2003). To determine evapotranspiration using satellite information, we can refer to several algorithms such as the surface energy balance system (SEBS) (Su 2002), surface energy balance (SEBAL) (Bastiaanssen et al. 1998), Surface Energy Balance Index (SEBI) (Menenti and Chudhury 1993), and Mapping Evapotranspiration at high Resolution with Internalized Calibration (Metric) (Allen et al. 2007).

The most commonly used models for estimating ET through satellite imagery are the SEBAL and SEBS algorithms. The SEBAL model was first developed by Bastiaanssen et al. (1998) and then improved by Allen et al. (2002). The SEBAL method has been widely used since its development in the western United States. Evapotranspiration has been estimated daily and monthly using this method (Kim et al. 2020). The surface energy balance model (SEBS) has been proposed by Su (2002) and includes a series of tools to determine the physical parameters of the earth's surface captured by satellite images (such as albedo, surface emission, surface temperature, vegetation index, etc.). The two algorithms of SEBS and SEBAL have been tested by researchers such as (Elhag et al. 2011; Bastiaanssen 1998; Elhag 2016; Gibson et al. 2014).

In fact, SEBS and SEBAL algorithms use satellite spectral observations and meteorological information to estimate energy fluxes and include a series of tools to determine the physical parameters of the earth's surface from satellite images such as albedo, surface emission, surface temperature, vegetation index, and etc. (Ferreira et al. 2016). Nowadays, the issue of enhancing product performance or increasing production per unit area is closely linked to the amount of water consumption, and water availability is a crucial factor in the agricultural industry. Therefore, it is necessary to study and assess water requirement and evapotranspiration of the plants in each region.

Kadem et al. (2014) used the FAO method and satellite images to estimate the rate of evapotranspiration. They obtained the rate of evapotranspiration for wheat by obtaining the indices (NDVI), albedo, and leaf area index required to estimate evapotranspiration. As a result, they used

lysimeter data to obtain the plant coefficient and its multiplication in evapotranspiration and obtained the rate of evapotranspiration. The results showed an estimate of 16.54% of the estimated values compared to the values obtained from the FAO. This is because of the use of low-pixel-density images to calculate the rate of evapotranspiration.

Gao et al. (2019) investigated the actual evapotranspiration using the SEBAL model on the Loess Plateau. The results of this study showed a direct relationship between the two parameters of vegetation and the rate of evapotranspiration. That is, the evapotranspiration rate of the region has increased with the increase of vegetation rate.

Shamloo et al. (2021) used the SEBAL model in estimating evapotranspiration and crop coefficient of corn in the Mediterranean region of Adana Province, Turkey. The outcomes displayed that the SEBAL algorithm could be a very convenient method since the performance of the SEBAL algorithm in estimating the actual evapotranspiration and crop coefficient using Landsat 8 satellite images is acceptable.

Losgedaragh and Rahimzadeghan (2018) compared the three methods of metric, SEBAL and SEBS to estimate the evapotranspiration of Amir Kabir Dam. The results showed that the metric and SEBS method had less error than the SEBAL method. Rahimzadeghan and Adehlsadat (2019) implemented the SEBAL model on pistachio crops in Semnan during 2013–2017 using 29 images of Landsat 8. The results showed high spatial variability of ET in the pistachio growth period. In general, the results show that the SEBAL model has a high efficiency for estimating the true ET of pistachio crops. Therefore, real evapotranspiration can be calculated periodically and regularly over a wide range of areas with high reliability. The amount of consumed water in crops can be measured by a hydrometer installation in any field of irrigation. However, high cost and low efficiency make this measurement a restrictive operational plan. In this regard, remote sensing has become a low-cost alternative with a real cover to meet water demand (Silva et al. 2018).

Most of the research that uses the SEBAL model evaluates the spatial and temporal distribution of ET by satellite sensors such as Landsat 5, Landsat 7, and Modis. However, only a handful of articles deal with ET estimation using Landsat 8, which launched in February of 2013 (Semmens et al. 2015; Senay et al. 2015) Also, the water requirement of agricultural areas and forests is often not studied. Water management is especially important in arid and semi-arid regions where precipitation is low and scattered. Currently, about 17% of the world's food requirements are produced by only 17% of the irrigated land (Abdullah 2006). However, irrigated agriculture faces serious threats such as water

shortage, degradation of land and water resources, unequal distribution, and limited access to water resources for irrigation (Rizvi et al. 2012).

Increasing population growth, development of agricultural lands in arid and semi-arid regions of the world, inconsistent distribution of freshwater in quantitative and spatial terms, as well as limitations and increasing quality problems of water resources in many countries like Iran, have turned providing reliable water supply to one of the fundamental challenges of the century. Damage caused by heat and water shortages to crops and orchards, including pistachios, is obvious (Karimi 2017).

According to the latest information published by the FAO, world pistachio production in 1997 was 331,403 tons. Among the countries of the world, ten countries each produced more than 250 tons of pistachios in 1997. Iran, ranking first, had a production of approximately 112,000 tons. Iran produces about 34% of the world's pistachios. After Iran, the United States is the second largest producer of pistachios in the world with a production of 82,000 tons. Recognizing the characteristics of pistachio trees in terms of their endurance and resistance to water shortage, it is possible to preserve the life of the tree and its production with the least amount of water. However, the tolerance of pistachio trees to water shortage, no matter what, is not a reason for the inherent nature of the tree as evidence has shown that pistachios, like other fruit trees, need a lot of water, and if during the growing season the plant reaches less-than-adequate water, the potential tree reaction has the opposite effect, and although it survives, its fertility and longevity are reduced (Naeini 2017).

Due to the problem of water shortage in the study area, the purpose of this study is to achieve three points: (1) Monitoring the real evapotranspiration using SEBAL and SEBS methods with the help of Landsat 8 images in agricultural areas, (2) Investigating the evapotranspiration potential of pistachio orchards using different experimental methods, (3) Determining water demand by crop is very important in irrigation systems.

Finally, the water requirements of pistachio crops in the study area are calculated, and the findings of this study will provide useful information for agricultural water management in the arid region of Dehshir that agricultural water management (AWM) includes the management of water used in crop production (both rainfed and irrigated), livestock, and inland fisheries to sustain food production, while preserving natural resources (Srivastava et al. 2021; Dube et al. 2023).

An important factor in this study is that the estimations are performed at different stages of the growth period. In other words, the hydro meteorological parameters driving

evapotranspiration would change as the plants are at different stages of maturity.

2 Materials and Methods

2.1 Study Area

Taft city is located in the southwest of Yazd province and due to the presence of Shirkuh mountain, the weather there is colder than the surrounding. The city of Taft generally consists of two parts: The northern part and the southern part, which are called warm and cold, respectively. One of the villages of Taft is Dehshir village. This village, together with 14 neighboring villages, forms Dehshir rural district. Dehshir climate has cold and relatively humid winters and warm to semi-temperate summers. The average annual temperature is about 14 degrees, which has varied between a maximum of 39 degrees and a minimum of -21 degrees during the statistical period. The average annual rainfall was about 130 mm, which varied between less than 50 mm to more than 300 mm (Fattahi

and Mehrshahi 2018). Due to the environmental conditions of the study area, most people are farmers and gardeners. Agriculture in the region is mostly drip and flood irrigation and the people of the region use groundwater to irrigate their crops Fig. 1.

2.2 Methods

In this study, in order to estimate the crop water stress of pistachio crops in Dehshir, Yazd Province, Landsat satellite (OLI) measurement products and meteorological data of the region in the water year 2018–2019 have been used. Landsat is an American satellite that was launched on February 11, 2013. Landsat 8 is the eighth satellite in the Landsat series and the seventh satellite in this project that successfully launched into orbit. This satellite, originally called (LDCM⁵), is a collaboration between NASA and the United States Geological Survey that was developed by Orbital Science Corporation. The NASA Goddard Space Flight Center is responsible for engineering development and orbiting satellites, and the US Geological Survey has developed ground systems and led the project. These

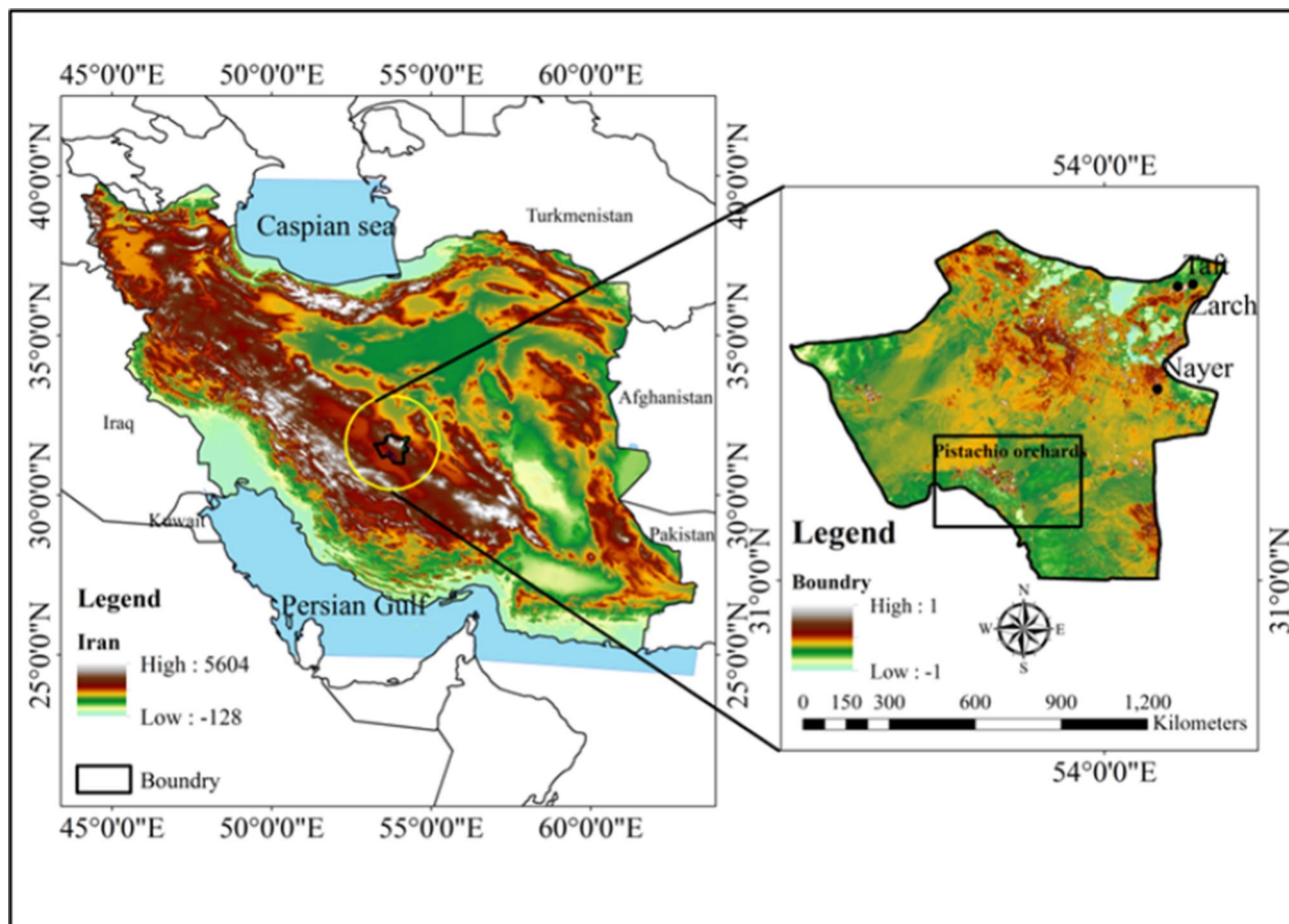


Fig. 1 Geographical location of the study area

Table 1 Multispectral bands of Landsat 8

Band names	Landsat 8 OLI	Spectral range (μm)	Spatial resolution(m)
Coastal aerosol	Band1	0.43–0.45	30
Blue	Band2	0.45–0.51	30
Green	Band3	0.53–0.59	30
Red	Band4	0.64–0.67	30
NIR	Band5	0.85–0.88	30
SWIR 1	Band6	1.57–1.65	30
SWIR 2	Band7	2.11–2.29	30
Pan	Band8	0.50–0.68	15
Cirrus	Band9	1.36–1.38	30

sensors provide images with an average resolution of 15 m to 100 m above the ground and the polar regions (Table 1).

The images used in this study have suitable meteorological conditions without clouds. Satellite data can be extracted from the Active Surface Process Distribution Archive Center of NASA (National Aeronautics and Space Administration) (<https://earthexplorer.usgs.gov/>). After taking the images, all the data for the study area will be mosaiced with the help of specialized software (GIS - Geographical Information System), ENVI (The Environment for Visualizing Images) and with the Universal Transverse Mercator Project System using the nearest-neighbor resampling method will be the nearest neighbor of geo-reference. Then the real evapotranspiration for the area will be calculated using the SEBAL and SEBS models. Then, due to the lack of facilities for ground measurement of evapotranspiration in the region, with synoptic data of the study area using 12 experimental methods, the potential evapotranspiration will be investigated (Fig. 2), and then the water requirement of the pistachio tree will be calculated.

2.3 Estimation of Production and Plant Parameters in SEBAL and SEBS Algorithms

The main inputs related to the SEBAL and SEBS models consist of remotely sensed biophysical parameters, including land surface temperature (LST or T_s), emissivity, normalized difference vegetation index (NDVI), and albedo, along with hourly meteorological parameters such as air temperature, wind speed, radiation, and relative humidity. In this study, the normalized difference of the Vegetation Index (NDVI) was calculated as below (Cosh et al. 2007):

$$\text{NDVI} = \frac{\rho_{\text{NIR}} - \rho_{\text{VIS}}}{\rho_{\text{NIR}} + \rho_{\text{VIS}}} \quad (1)$$

In this formula, ρ_{NIR} is the reflection in the near-infrared band (1.725/1.1 μm) and ρ_{VIS} is the reflection in the visible band (68–58 μm). The range of NDVI values varies from -1 to +1. High reflection in the near-infrared part of the electromagnetic spectrum indicates the health of the plant with large values between 0.5 and 1 (Lillesand and Keifer 1994).

2.4 LST Estimation in SEBAL and SEBS Algorithms

Temperature determination in satellite images is calculated through a separate window (SWT⁶). A split-window technique is one of the methods for determining the surface temperature, which is used first to determine the sea surface temperature and then to calculate the surface temperature. To use this method, it is necessary to have a spectral band in the thermal infrared range. The general principles of this method are based on the difference in atmospheric transmission in two adjacent spectral ranges in the infrared region between the 11- and 12- μm spectra. As the effect of the atmosphere on different wavelengths varies, this factor creates a framework difference in the separate window method used to calculate the temperature. One of the effective parameters in this method is to determine the amount of emission at the surface, the amount of which for seawater is assumed 1, therefore, the calculation of sea surface temperature is done with great care using this method, but in estimating the earth's surface temperature, the emissivity changes were considered in the algorithm. The emissivity value is a function of the amount and density of vegetation and vegetation indices should be used to calculate it (Kerr et al. 2004). In total, different methods are presented using a Split Window Technique, and method (SWT) is as follows in Eq. (2):

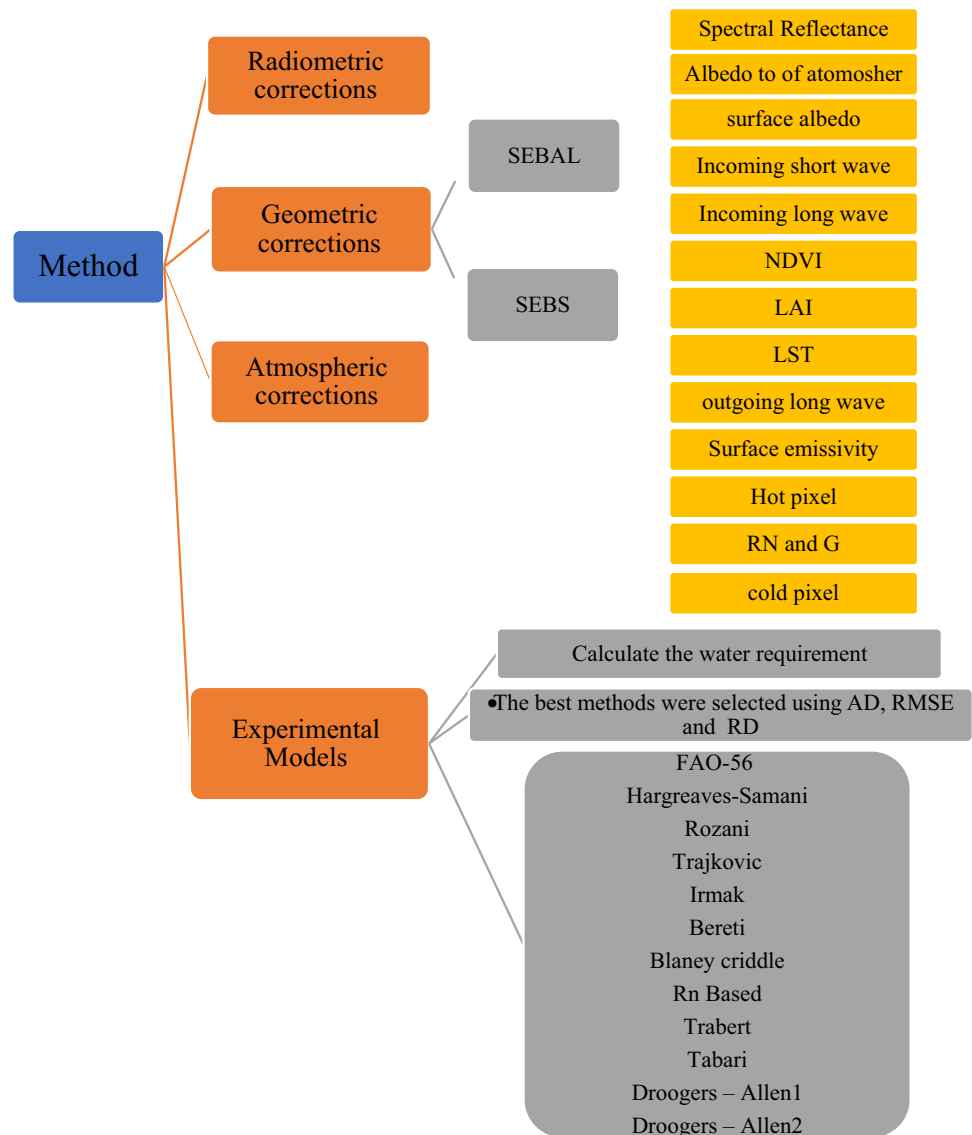
$$T_s = T_i - C1(T_i - T_j) + C2(T_i - T_j)2 + C0 + (C3C4W)(1 - \epsilon) + (C5 + C6W)\Delta\epsilon \quad (2)$$

In the method (SWT) the land surface temperature (LST) is expressed as (T_s); that T_i and T_j are the temperatures of the sensor lighting in separate T_i and T_j window bands (Kelvin), ϵ ; average emission, $\epsilon = 0.5(\epsilon_i + \epsilon_j)$ $\Delta\epsilon$; emission difference $\Delta\epsilon = (\epsilon_i - \epsilon_j)$, w ; total amount of atmospheric water (g/cm^2) and c_0 - c_6 ; coefficients of window algorithm obtained from simulated data (Kerr et al. 2004; Younesszadeh Jalili 2013).

2.5 SEBAL Algorithm

The SEBAL model calculates the amount of evapotranspiration using satellite images and minimum ground

Fig. 2 Flowchart of research methods



station data required based on the energy balance equation. Since satellite images can only provide data about the satellite's transit time, SEBAL can calculate the amount of evapotranspiration flux for each pixel of the image as the remainder of the surface energy balance equation (Bastiaanssen 1995). The general equation of the energy balance algorithm is given in Eq. (3) below.

$$R_n = G + H + \lambda ET \tag{3}$$

where R_n is the total radiation flux in terms of (W/m^2), λET : is the amount of latent heat flux at the moment of satellite transit in terms of (W/m^2), H : is sensible heat flux of air in terms of (W/m^2); G : is the soil heat flux in terms of (W/m^2) the total radiation flux is the algebraic calculation between all the input radiation and the output reflectance. Total radiation flux is the algebraic sum of short-wavelength radiation

as a function of surface albedo and long-wavelength radiation obtained from the difference between the input and output long wavelengths. The amount of short-wavelength radiation coming out of the ground is about 3–100 μm and the total radiation flux is also calculated using Eq. (4):

$$R_n = (1 - \alpha)R_{s\downarrow} + R_{L\downarrow} - (1 - \epsilon_o)R_{L\uparrow} \tag{4}$$

In it, R_n total radiation flux in terms of $R_{s\downarrow}$ (W/m^2) short-wave radiation, α surface albedo without dimension, $R_{L\downarrow}$ longwave radiation, $R_{L\uparrow}$ long wave reflection, ϵ_o ability to propagate surface without dimension.

2.6 Soil Heat Flux

Soil heat flux is the amount of soil storage as a result of the temperature gradient between the soil surface and the lower

soil layers. The temperature gradient is a function of vegetation and leaf area index (LAI), which expresses the heat ratio of the bare soil surface by preventing light from entering the soil surface and forming a shadow above the bare soil. Since field information on soil thermal conductivity is not available, experimental relationships include a function of vegetation index, surface albedo, and surface temperature are used to calculate soil heat flux.

Soil heat flux is calculated using Eq. (5) proposed by Bastiaanssen (1995).

$$\frac{G}{R_n} = T_s/\alpha(0.0038\alpha + 0.0074\alpha^2)(1 - 0.98NDVI^4) \quad (5)$$

T_s : Surface temperature in degrees Celsius, α : Surface albedo, NDVI: Vegetation Index.

2.7 Perceptible Heat Flux

Perceptible heat flux is the amount of energy loss from the soil through the interconnection and the diffusion process as a result of the temperature difference between the surface and the lowest layer of the atmosphere. Perceptible heat flux is a major obstacle in estimating evapotranspiration, as the value of dT terms and the aerodynamic resistance of the surface are unknown to calculate the perceived heat flux. Perceived heat flux is a major obstacle in estimating evapotranspiration, because the value of dT terms and the aerodynamic resistance of the surface are unknown to calculate the perceptible heat flux. To calculate these unknowns of the algorithm, the sensible heat flux is calculated in dry and wet pixels first. Dry or hot pixels should be selected in the dry and barren area where evaporation does not occur. Cold or wet pixels must have a surface temperature that is the same as the air temperature. Internal calibration of sensible heat flux algorithm by the SEBAL algorithm eliminates the need for atmospheric correction by radiant models to calculate surface temperature and albedo. This internal calibration also reduces the effects of error in estimating roughness coefficients and aerodynamic strength. According to the determination of hot and cold pixels, a linear relationship is established between the dT term and the surface temperature. The sensible heat flux is calculated using Eq. (6).

$$H = (P \times C_p \times dT)/r_{ah} \quad (6)$$

P: Air density in terms of (kg/m³), C_p : Specific air heat equal to 1004 (J / kg /K), dT: Temperature difference between two heights Z_1, Z_2 in term of (K), r_{ah} : Aerodynamic resistance to heat transfer (s/m).

2.8 Latent Heat Flux

The latent heat flux is the algebraic difference of the energy balance equation. After calculating the latent heat flux, the evaporative component is determined. Applying the evaporative component per pixel, the amount of evapotranspiration in 24 h is calculated. Instant evapotranspiration is obtained using Eq. (7).

$$ET_{inst} = 3600 \frac{\lambda ET}{\lambda} \quad (7)$$

Here, ET is the amount of instantaneous evapotranspiration in terms of (mm/h), λ the latent heat flux or the amount of heat absorbed in evaporation of 1 kg of water in terms of (J/kg) (Waters et al. 2002).

2.9 SEBS Algorithm

In the following, we will briefly introduce the SEBS algorithm. The basis of this method is using the energy balance equation (Eq. 8) to calculate the amount of latent heat flux of evaporation as the remainder of this equation for each pixel.

$$\lambda ET = R_n - G - H \quad (8)$$

In this equation, λET is the latent heat flux of evaporation in terms of (W/m²), R_n is the amount of pure solar radiation in terms of (W/m²), and G is the heat flux of the soil in terms of (W/m²) and H is the tangible heat flux in terms of (W/m²). The amount of pure solar radiation (R_n) is calculated using the surface radiation balance equation (Eq. 9).

$$R_{swd} + \varepsilon R_{lwd} - \varepsilon \sigma T_0^4 R_n = (1 - \alpha) \quad (9)$$

In this equation, α is the surface albedo, R_{swd} is the input shortwave radiation in terms of (W/m²) (ε surface emission, Stephen constant = Boltzmann constant (5.67×10^{-8} W/m²/K⁴) and T_0^4 is surface temperature. In arid and semi-arid regions, the lack of vegetation causes the effects of ground soil reflection to overcome the effect of vegetation reflection. SAVI, which is the corrected NDVI index, reduces the effects of base soil and soil moisture on the NDVI index and is calculated through Eq. (10).

$$SAVI = \frac{(1 + L)(\rho_4 - \rho_3)}{(\rho_4 + \rho_3 + L)} \quad (10)$$

ρ_3, ρ_4 are spectral reflectance of 3, 4, and L is the correction factor of soil effects, the range of which is from zero for compressed vegetation and 1 for low-density vegetation. This factor is calculated from Eqs. (11) and (12) using image information.

$$L = 1 - 2 \times a \times NDVI \times WDWI \quad (11)$$

$$\text{WDVI} = \rho_4 - \gamma \rho_3 \quad (12)$$

In Eqs. (11) and (12), $a = 1.6$, γ are the soil coefficient, which is actually the slope of the fitted line on the spectral reflectance diagram of the near-infrared bands (band 4) and the red band (band 3) (Yang et al. 2006). In this equation, a new method has been used to calculate the surface albedo that applies atmospheric corrections to all bands of the sensor (13). Surface albedo is estimated using Eqs. (14)–(16).

$$\rho_{s,b} = \frac{\rho_{t,b} - \rho_{a,b}}{\tau_{in,b} \cdot \tau_{out,b}} \quad (13)$$

where $\rho_{s,b}$ reflection rate in each band of the sensor at the surface (dimensionless), $\rho_{t,b}$ reflection in each band of the sensor above the atmosphere (dimensionless), $\rho_{a,b}$ is a constant value of false reflection for each band (no dimension), τ_{in} , atmospheric transmittance for incoming solar radiation in each band calculated from Eq. (15), τ_{out} , atmospheric transmittance for output radiation reflected from the surface at each of the band is calculated from Eq. (16).

$$\rho_{t,b} = \frac{\pi \cdot L_b}{\text{ESUN}_b \cdot \cos \theta \cdot d_r} \quad (14)$$

In this equation, ESUN_b is the solar radiation potential in each band, θ is the angle of solar radiation, d_r is the inverse of the relative distance between the earth and the sun, and L_b is the spectral radiation of each band.

$$\tau_{in,b} = c_1 \exp \left[\frac{C_2 \cdot P_{air}}{K_t \cdot \cos \theta_h} - \frac{C_3 W + C_4}{\cos \theta_h} \right] + C_5 \quad (15)$$

$$\tau_{out,b} = c_1 \exp \left[\frac{C_2 \cdot P_{air}}{K_t \cdot 1} - \frac{C_3 W + C_4}{1} \right] + C_5 \quad (16)$$

C^1 – C^5 is the generalized coefficients of the MODTRAN (the MODerate resolution atmospheric TRANsmission model) (Van der Tol et al. 2009 (model for each band (17), P_{air} is average atmospheric pressure (KP_a), W is the hovering water in the atmosphere, K_t is the opacity coefficient, which is considered to be 1. θ_h in Eq. (10) is angles of sunlight from the horizon surface and in Eq. (17) is sensing angles from the horizon surface (zero for Landsat images).

$$\alpha = \sum_{b=1}^7 \rho_{s,b} \cdot W_b \quad (17)$$

α is the albedo of the surface W_b , is the weighting coefficients for each band. Soil heat flux in the SEBS algorithm is obtained from Eq. (18).

$$G_0 = R_n \cdot [\bar{\Gamma}_c + (1 - f_c) \cdot (\bar{\Gamma}_s - \bar{\Gamma}_c)] \quad (18)$$

In this equation, $\bar{\Gamma}_c$ is the ratio of soil heat flux to net radiation for dense vegetation is considered to be 0.05. $\bar{\Gamma}_s$ is ratio of soil heat flux to net radiation for bare soil is considered to be 0.315. f_c is a partial canopy coverage that can be calculated using remote sensing data (19).

$$f_c = \left(\frac{\text{NDVI} - \text{NDVI}_{\min}}{\text{NDVI}_{\max} - \text{NDVI}_{\min}} \right)^2 \quad (19)$$

In this equation, NDVI_{\max} , NDVI_{\min} , and NDVI are the values of NDVI in pixels containing dense vegetation, bare soil, and current pixels, respectively (Temesgen 2009). Perceptible heat flux is the heat energy transferred between the surface and the air. In SEBS model, Manin-Abukov (Brutsaert 1982) conditions are used to calculate the sensible heat flux in Eq. (20, 21)

$$u = \frac{u_*}{k} \left[\frac{\ln \left(\frac{z - d_0}{z_{om}} \right)}{-\psi_m \left(\frac{z - d_0}{L} \right) + \psi_m \left(\frac{z_{om}}{L} \right)} \right] \quad (20)$$

$$\theta_0 - \theta_m = \frac{H}{k u_* \rho c_p} \left[\frac{\ln \left(\frac{z - d_0}{z_{oh}} \right)}{-\psi_m \left(\frac{z - d_0}{L} \right) + \psi_h \left(\frac{z_{oh}}{L} \right)} \right] \quad (21)$$

In this equation, z is the reference height (m), u is the wind speed and u_* is the friction velocity (m/s), d_0 is the displacement height (m), z_{om} and z_{oh} is the roughness height for momentum and heat transfer (m), $k = 0.4$ van Carmen fitted, C_p is the dry weather's heat condition (J/kg) ρ is the air density (kg/m^3), θ_0 , θ_a potential surface temperature and air temperature at altitude, z ψ_h and ψ_m Stability correction factor for momentum and atmospheric heat transfer, L is the length of Abukov (m) defined as Eq. (22).

$$L = - \frac{\rho u_*^3 c_p \theta_v}{kgH} \quad (22)$$

In this equation, g is the acceleration of gravity (m/s^2) and θ_v is the virtual temperature near the surface (k). The roughness length for momentum (Z_{om}) transfer is the height above the zero displacement surface. Level zero for wind profiles starts at ground level or vegetation. Z_{om} calculated with Eq. (23).

$$z_{om} = \exp \left[\left(a \times \frac{\text{NDVI}}{a} \right) + b \right] \quad (23)$$

In this equation, a and b are fixed values of the equation that are determined by regression between the values (NDVI/a) and Z_{om} in two or more pixels of the specified plant index. (Morse et al 2000). The roughness length for heat transfer Z_{oh} is estimated using Eq. (24) (Su 2002).

$$z_{oh} = \frac{z_{om}}{\exp(KB^{-1})} \tag{24}$$

In this equation, KB^{-1} , the Stanton number shows the additional resistance to heat transfer that is calculated by (Su et al. 2010) Eq. (25).

$$KB^{-1} = \frac{KC_d}{4C_t \frac{u_*}{u(h)} (1 - e^{-ne/e/2})} f_c^2 + 2f_c f_s \frac{k \cdot u_* / u(h) \cdot z_{om} / h}{C_t^*} + KB_s^{-1} f_s^2 \tag{25}$$

in which C_d is the leaf drag coefficient of the trees, which is assumed to be 0.2, f_c is the partial canopy cover and f_s is the complement f_c , C_t is the heat transfer coefficient from the leaf, which for most canopies and environmental conditions is between 0.005 N and 0.075 N. N demonstrates number of sheets involved in heat exchange and KB_s^{-1} for bare soil obtained from Eq. (26).

$$KB_s^{-1} = 2.46(Re_*)^{1/4} - 1n[7.4] \tag{26}$$

where (Re_*) is the Reynolds roughness number for soil. Evaporation fraction in SEBS is obtained by using sensible heat flux. Under dry conditions, the latent heat flux is minimal and can be ignored, in this case the equilibrium equation is summed as Eqs. (27) and (28).

$$\lambda E_{dry} = R_n - G_0 - H_{dry} = 0 \tag{27}$$

$$or H_{dry} = R_n - G_0 \tag{28}$$

In wet conditions, the actual evapotranspiration reaches the potential evapotranspiration; in this case we have (29,30):

$$\lambda E_{wet} = R_n - G_0 - H_{wet} = 0 \tag{29}$$

$$or H_{wet} = R_n - G_0 - \lambda E_{wet} \tag{30}$$

H_{wet} is estimated in the Penman–Monteith relation using Eq. 31 (Su 2002).

$$H_{wet} = \left[(R_n - G_0) - \frac{\rho C_p}{r_{ew}} \cdot \frac{e_s - e}{\gamma} \right] / \left[1 + \frac{\Delta}{\gamma} \right] \tag{31}$$

The aerodynamic drag is obtained from Eq. (32) in wet conditions.

$$r_{ew} = \frac{1}{Ku_*} \left[\ln \left(\frac{z - d_0}{z_{oh}} \right) - \psi_h \left(\frac{z - d_0}{L_w} \right) + \psi_h \left(\frac{z_{oh}}{L_w} \right) \right] \tag{32}$$

Manin-Abukov length is obtained from Eq. (33) in wet conditions.

$$L_w = - \frac{\rho u_*^3}{kg \cdot 0.61 \cdot (R_n - G_0) / \lambda} \tag{33}$$

It λ has a latent heat of vaporization (2.45 MJ.kg⁻¹). The relative evaporation fraction is obtained using Eq. (34).

$$\Lambda_r = \frac{\lambda E}{\lambda E_{wet}} = 1 - \frac{\lambda E_{wet} - \lambda E}{\lambda E_{wet}} = 1 - \frac{H - H_{wet}}{H_{dry} - H_{wet}} \tag{34}$$

Finally, the evaporation fraction is obtained from Eq. (35).

$$\Lambda = \frac{\lambda E}{H + \lambda E} = \frac{\lambda E}{R_n - G_0} = \frac{\Lambda_r \cdot \lambda E_{wet}}{R_n - G_0} \tag{35}$$

Daily evapotranspiration (ET_a) is calculated from Eq. (36) assuming that the evaporation fraction is constant during the day:

$$ET_a = 8.64 \times 10^7 \times \frac{\Lambda \cdot R_{nday}}{\lambda \rho_w} \tag{36}$$

where ρ_w is the density of water in terms of (kg/m³), and R_{nday} is the net daily radiation in terms of (Wm²).

3 Experimental Methodology

3.1 Penman–Monteith Method FAO-56

The Penman–Monteith equation is summarized as Eq. (37):

$$ET_0 = \frac{0.408\Delta(R_n - G) + \gamma [890 / (T + 273) U_2 (e_a - e_d)]}{\Delta + \gamma (1 + 0.34U_2)} \tag{37}$$

where, ET_0 displays the reference crop evapotranspiration (mm / day), T stands for the average air temperature at a height of 2 m above ground level, U_2 shows the wind speed at a height of 2 m above ground level (ms⁻¹), $e_a - e_d$ is the vapor pressure deficit (KP_a), Δ is the vapor pressure curve slope ($KP_a C^{-1}$), and γ presents the Psychrometric coefficient ($KP_a C^{-1}$) (Bastiaanssen et al. 1998).

This part deals with the equations that used empirical methods. All meteorological variables are derived based on a monthly scale (sum). Here R_s shows the solar radiation in mm / day, T_c presents the average monthly temperature in °C, R_a is the radiation, T stands for the average daily air temperature, T_{max} displays the maximum monthly temperature, T_{min} is the minimum monthly

Table 2 Equations of experimental methods (Piri & Pozan, 2019)

Row	Method	Equations
38	Hargreaves-Samani	$(T_c + 17.8) = 0.0162 R_s ET_0 ET_0$
39	Rozani	$ET_0 = 0.408 \times (0.817 + 0.00022z) 0.0023 Ra (T_{mean} + 17.8) (T_{max} - T_{min})^{0.5}$
40	Trajkovic	$ET_0 = 0.408 \times 0.0023 Ra (T_{mean} + 17.8) (T_{max} - T_{min})^{0.424}$
41	Irmak	$ET_0 = 0.408 \times 0.00193 Ra (T_{mean} + 17.8) (T_{max} - T_{min})^{0.5}$
42	Bereti	$ET_0 = 0.408 \times 0.00193 Ra (T_{mean} + 17.8) (T_{max} - T_{min})^{0.5}$
43	Blaney-Criddle	$ET_0 = P(0.46T_{mean} + 8.17)$
44	Rn Based	$ET_0 = 0.289R_s + 0.023T_{mean} + 0.489$
45	Trabert	$ET_0 = 0.408 + 0.00193 Ra (T_{mean} + 17.8) (T_{mean} + 17.8) (T_{max} - T_{min})^{0.517}$
46	Tabari	$ET_0 = -0.642 + 0.174R_s + 0.0353Ta$
47	Droogers – Allen1	$ET_0 = 0.408 \times 0.0030 Ra (T_{mean} + 17.8) (T_{max} - T_{min})^{0.5}$
48	Droogers – Allen2	$ET_0 = 0.408 \times 0.0025 Ra (T_{mean} + 16.8) (T_{max} - T_{min})^{0.5}$

temperature, and P is the sunshine hours (Table 2) (Piri and Taher 2019).

Finally, the crop coefficient for the understudy pistachio fields was derived via monthly SEBAL and SEBS ET (ET_{mon}) and monthly ET₀

$$Kc = ET_{mon}/ET_0, mon \quad (49)$$

3.2 Investigating the Error of Experimental and Actual Methods

$$RD = \left| \frac{X_i - X_m}{X_m} \right| \quad (50)$$

$$RMSE = \sqrt{\frac{\sum_{i=1}^n (X_i - X_m)^2}{n}} \quad (51)$$

$$AD = X_i - X_m \quad (52)$$

RD relative difference, RMSE root-mean-square error, AD absolute difference.

where X_i is evapotranspiration that is calculated using the SEBS and SEBAL algorithm, X_m is evapotranspiration which is calculated using experimental methods and n is the number of evapotranspiration data in the Eqs. (50, 51, 52) (Hyndman and Koehler 2006).

4 Results and Discussion

4.1 Vegetation (NDVI)

Vegetation maps of the study area were prepared by the OLI satellite for a 1-year statistical period (2018–2019) separately for each month. NDVI followed a constant pattern through the study and dates. In spring (April, May, June) and summer (July, August, September), the maximum values of NDVI in pixels are between 0.4 and 1, which is higher than other months because the growing season begins and vegetation turns into its high case in both spring and summer. In autumn (October, November, December) and winter (January, February, and March) NDVI decreased due to harvesting and crop senescence (Fig. 3). As the maps present, the density and spatial distribution of the vegetation show large variations from one month to another, which in turn indicates the vegetation dynamics of this area and the effect of environmental and climatic factors on them.

4.2 Land Surface Temperature

The seasonal patterns were also followed by LST, as LST values were lower (299.75 K, 25.26 °C) in January and higher in August (334 K, 58 °C). In general, gardens and agricultural lands have a lower surface temperature due to vegetation. Since the plant type and the vegetation canopy can influence and vary the micro-climate at the soil surface below a vegetation canopy (eco-climate), the existence of vegetation decreases airflow and the vegetation shadow covers the soil surface (Fig. 4).

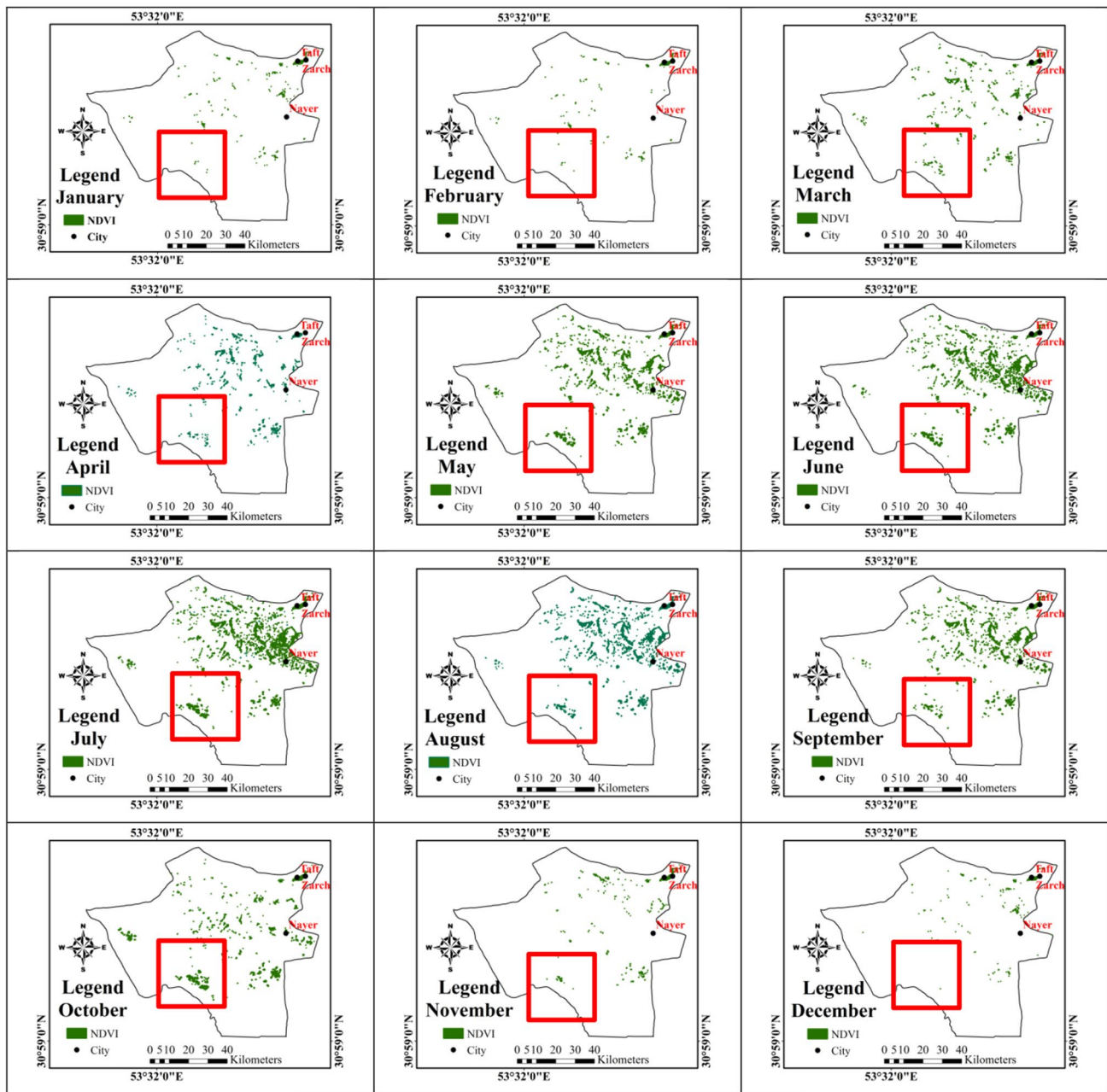


Fig. 3 NDVI images extracted from Landsat 8 images

4.3 Potential ET from Empirical Methods

PET from the above-mentioned 12 empirical methods revealed that the lowest rate of evapotranspiration is in January. It was found that the temporal pattern was similar, as values from most models were maximum during the months of August and July. In most cases, the highest rate of PET

was achieved by the H–S, Blaney-Cridde, Rn-based, and Trabert methods. For July, as the key irrigation season, H–S, Blaney-Cridde, Rn-based, and Trabert methods estimated that PET was 256.38, 212.52, 131.82, and 210.34 mm. The lowest rate of evapotranspiration was estimated by Trajkovic, Bereti, and Tabari methods in the Dehshir Plain in Fig. 5.

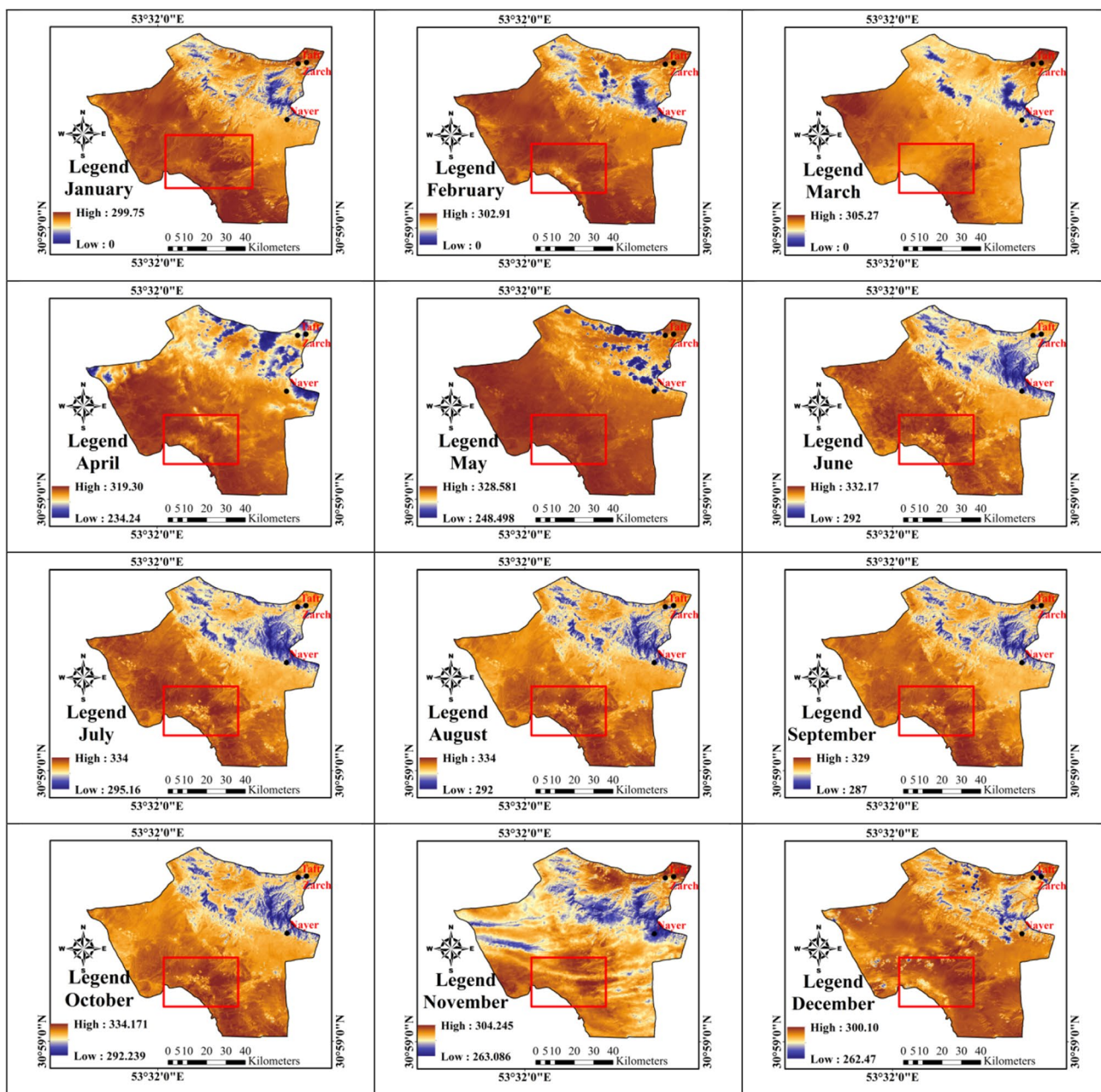


Fig. 4 LST images extracted from Landsat 8 images (Kelvin)

4.4 Evapotranspiration Using the SEBAL Method

ET values were higher in spring and summer across the vegetated area for the under study region (Fig. 6), which shows that SEBAL-derived monthly ET followed seasonal patterns. This is mainly due to the increased solar radiation and enhanced vegetation growth. The spatial variability of monthly ET across the investigated area happens because of variations in the date when the growing season starts and ends. Monthly SEBAL ET was found to be the maximum range during the peak growing season (July and August) at

around 376 and 320 mm, when the vegetation reached its maximum greenness ($NDVI=0.4-1$). When the peak growing season ended, ET values decreased in the 3 months of winter as a result of decreasing plant density and decreasing temperature and the reduced demand for water (Fig. 6).

4.5 Evapotranspiration Using the SEBS Method

SEBS-derived monthly ET followed seasonal patterns like those derived via SEBAL, since ET values were higher in spring and summer across the vegetated area for the regions

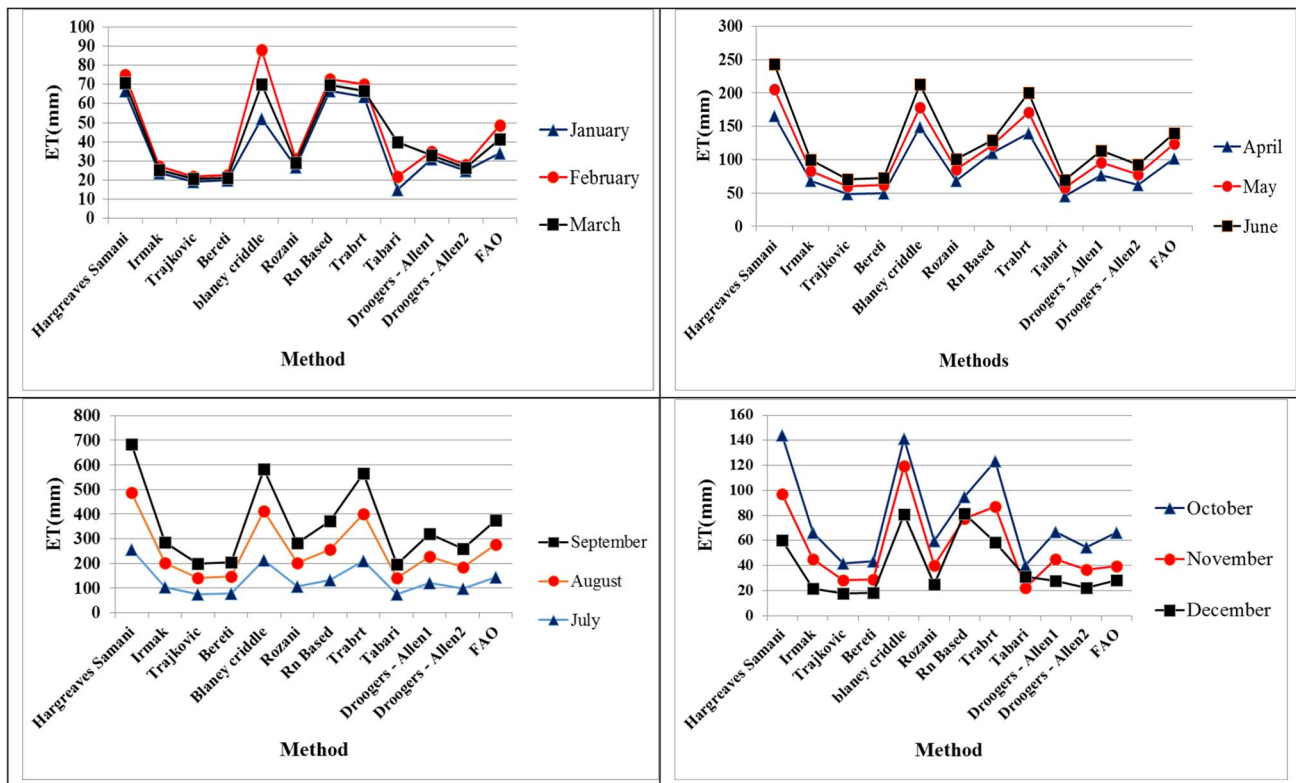


Fig. 5 Evapotranspiration diagram prepared by experimental methods

understudy (Fig. 7). This is largely due to the increased solar radiation and enhanced vegetation growth. The spatial variability of monthly ET across the study area happens because of the variations in crop type and the date when the growing season begins and ends. Monthly SEBS ET was found to be the maximum range during the peak growing season (July and August) at around 243.27 and 237.54 mm, when the vegetation reached its maximum greenness (NDVI=0.4–1). When the peak growing season ended, ET values decreased in the 3 months of winter with decreasing plant density and decreasing temperature and the reduced demand for water. It is important to mention that the calculated evapotranspiration rate of pistachio by SEBS method is less than SEBAL method (Fig. 7).

4.6 Comparison Between SEBAL and SEBS Algorithm with Empirical Models

For this purpose, we have used AD, RD, and RMST statistics in order to examine the accuracy of different empirical methods compared to SEBS and SEBAL algorithms. In accordance with AD method, the difference between actual monthly ET based on SEBAL and SEBS, and the PET¹ based on the empirical models algorithm was found to be in its maximum rate in July and August (in summer) and

its minimum rate in January in winter, respectively. This pattern was consistent across all models; however, the difference between actual and potential ET was much larger in August (e.g., from Trajkovic method, SEBS and SEBAL were 170,153 mm respectively, and from Tabari they were 170, 152 mm, respectively); their difference was minor in February (e.g., from the H–S method, SEBS and SEBAL were 7,14 mm, respectively). The reason for the large difference in August and July is that, during this peak growth period of pistachio trees, the vegetation density increased.

The comparison between ET₀ from the empirical models against the SEBAL and SEBS algorithms methods recommends that H–S, Blaney-Criddle, Rn-based, and Trabert may be the most suitable models among the 12 models.

It is recommended that H–S, Blaney-Criddle, Rn-based, and Trabert may be the most suitable models among the 12 models. For example, in Table 3, the difference between SEBAL and SEBS algorithms methods with approved empirical methods is stated, for instance, in July, August and September, the difference between the HS and SEBS methods is stated as 13, 6, and 31 mm. The difference between SEBAL and HS algorithms methods, for example, in July,

¹ potential evapotranspiration.

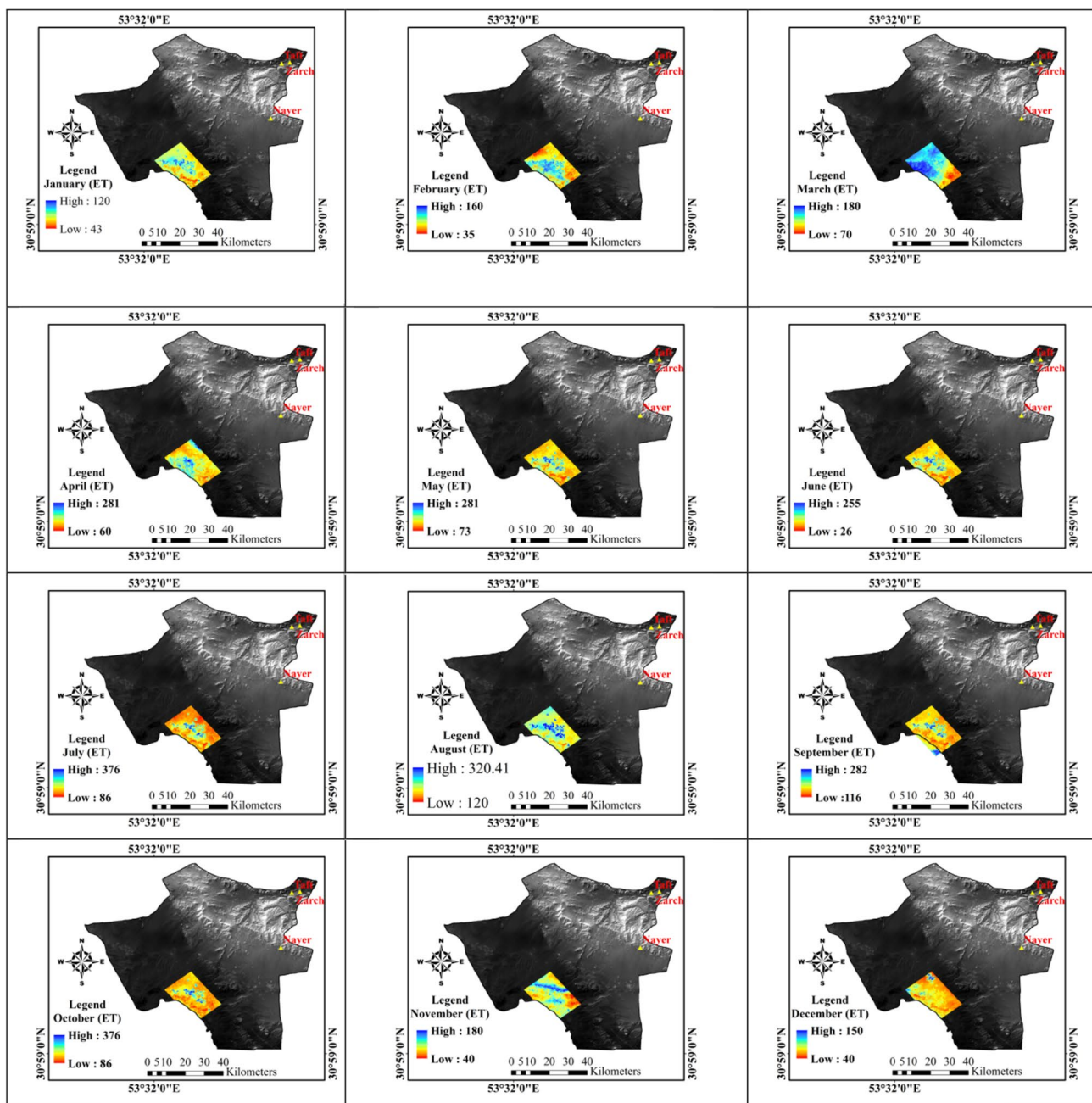


Fig. 6 Evapotranspiration images prepared using SEBAL method from Dehshir pistachio orchards

August and September is stated as 25.3, 11.8, and 31 mm. Three other approved methods are presented in Table 3.

On the other hand, Trajkovic, Bereti, Tabari, Droogers–Allen1, Droogers–Allen2, and Rozani methods models were identified as the non-applicable methods with large AD (Fig. 8, Table.3).

RD statistics have been used to investigate the accuracy of different empirical methods and to compare them with SEBS and SEBAL algorithms. According to RD method, the difference between actual monthly ET based on SEBAL

and SEBS, and the PET² on the based on empirical models algorithm were maximum in March and August and minimum in January in winter, respectively. This pattern was consistent across all models; however, the difference between actual and potential ET was much larger in the Trajkovic, Bereti, Tabari, and Rozani methods (e.g., in August, from Trajkovic method, SEBS and SEBAL were

² potential evapotranspiration.

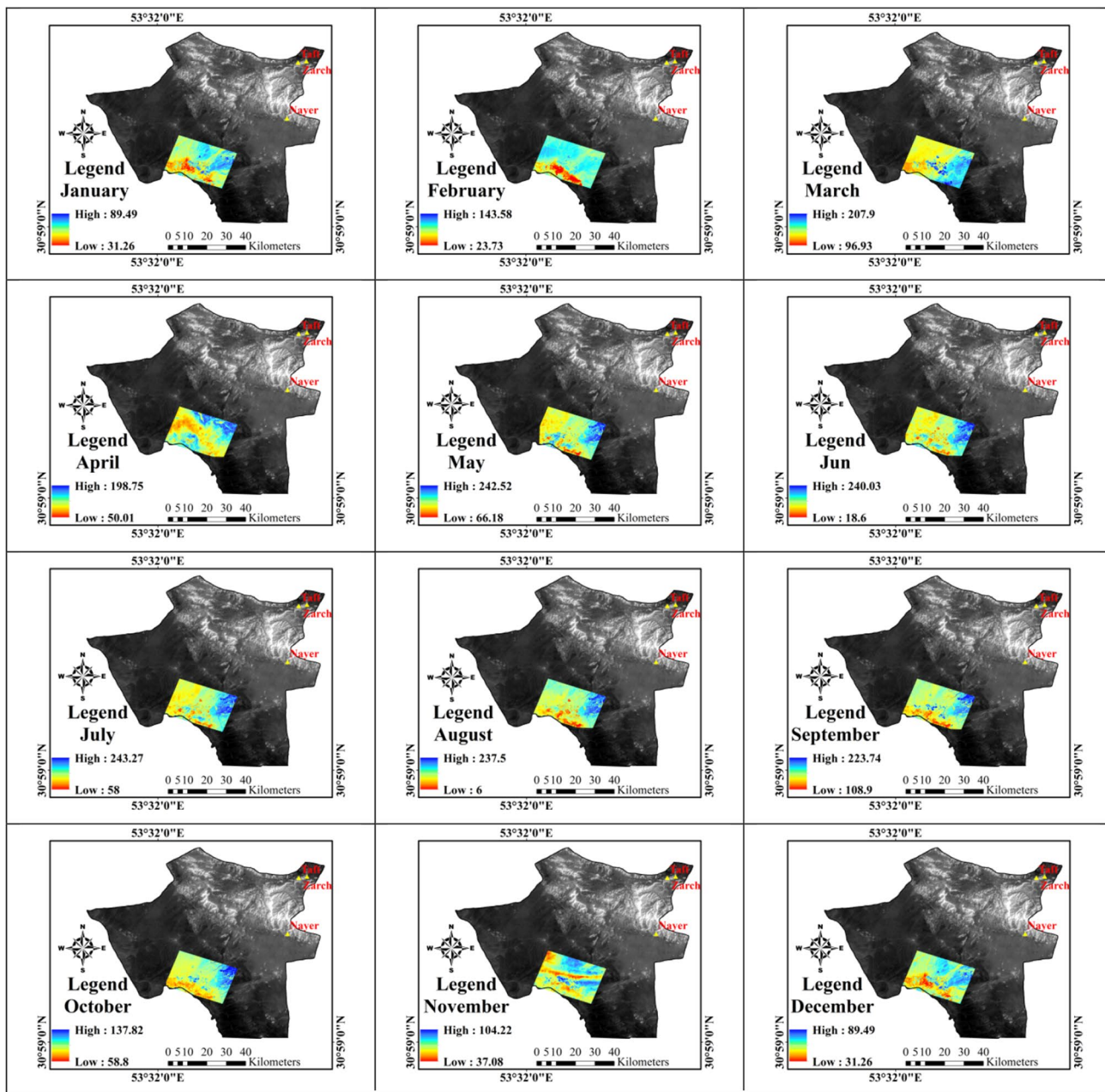


Fig. 7 Images of evapotranspiration prepared using SEBS method from Dehshir pistachio orchards

2.5 and 2.27 mm respectively, and from Tabari, they were 2.5, 2.24 mm respectively); the difference was minor in the H–S, Blaney-Criddle, Rn-based, and Trabert methods (e.g., 0,0.05 mm for SEBS and SEBAL, respectively, from the H–S method).

Comparison of ET_0 from the empirical models against the SEBAL and SEBS algorithms methods suggest that

H–S, Blaney-Criddle, Rn-based, and Trabert may be the most suitable models among the 12 models.

In Table 4, the difference between SEBAL and SEBS algorithms methods with approved empirical methods, for example, in July, August, and September is stated as 0.1, 0, and 0.2 mm; the difference between the HS and SEBS methods is stated; and the difference between SEBAL and HS algorithms methods for example, in July, August, and

Table 3 Difference between potential evapotranspiration (Trabert, Rn-based, B-C, H-S) and real evapotranspiration (SEBS and SEBAL) in summer

Methods	July	SEBS	August	SEBS	September	SEBS	July-SEBS	August-SEBS	September-SEBS
H-S	256.3	243.2	231.8	237.4	196.6	165.8	13	6	31
B-C	212.5	243.2	199.5	237.4	171.4	165.8	31	38	6
Rn-based	131.8	243.2	124.3	237.4	114.7	165.8	111	113	51
Trabert	210.3	243.2	191.3	237.4	164.4	165.8	33	46	1

Methods	July	SEBAL	August	SEBAL	September	SEBAL	July-SEBAL	August-SEBAL	September-SEBAL
H-S	256.3	231	231.8	220	196.6	199	25.3	11.8	2.3
B-C	212.5	231	199.5	220	171.4	199	18.4	20.4	27.5
Rn-based	131.8	231	124.3	220	114.7	199	99.1	95.6	84.2
Trabert	210.3	231	191.3	220	164.4	199	20.6	28.6	34.5

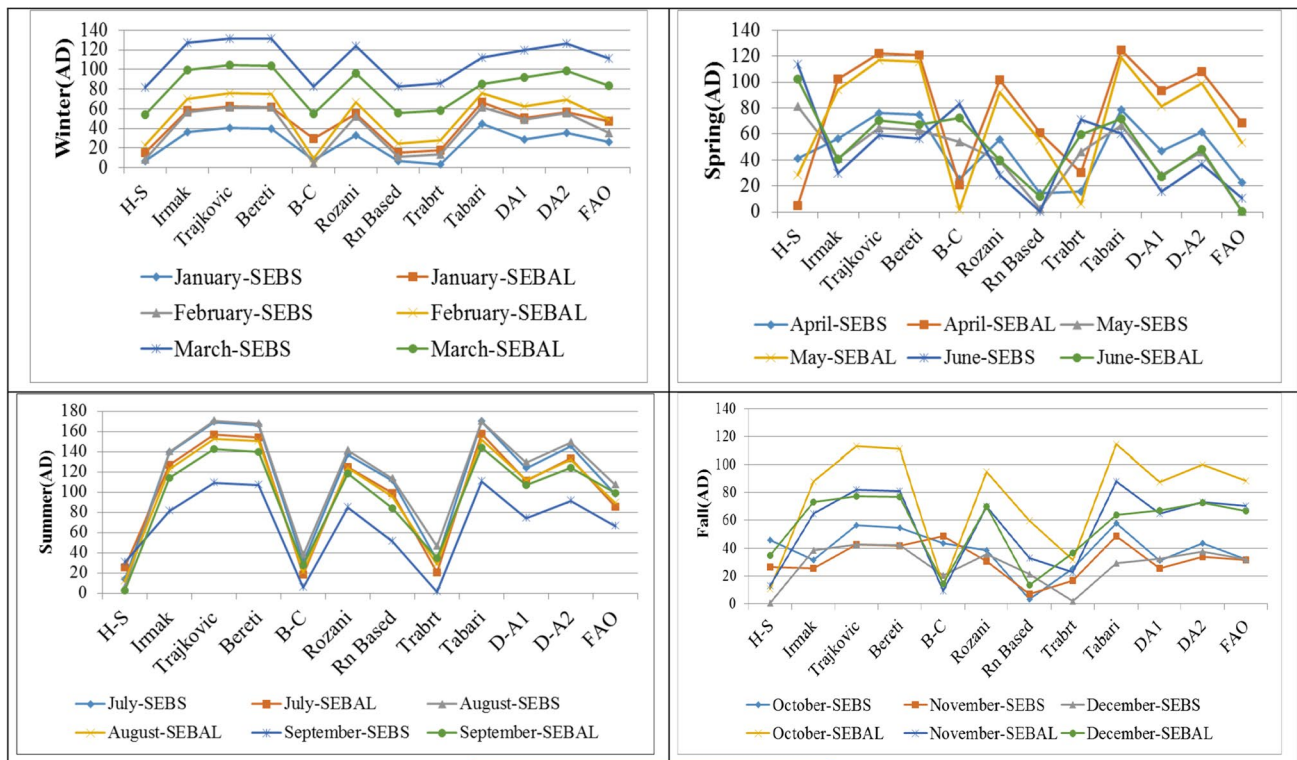


Fig. 8 Calculated error rate (AD)

September is stated as 0.1, 0.05, and 0.01 mm. Three other approved methods are presented in Table 4.

On the other hand, Trajkovic, Bereti, Tabari, Droogers–Allen1, Droogers–Allen2, and Rozani methods models were identified as the unsuitable methods with large RD. As expected, RD of ET_0 from all models was maximum

during the month of August and minimum in January (Fig. 9, Table 4).

According to the RMSE method, Comparison of ET_0 from the empirical models against the SEBAL and SEBS algorithms methods suggest that H-S, Blaney-Cridde, Rn-based, and Trabert may be the most suitable models among the 12 models. On the other hand, Trajkovic, Bereti, Tabari,

Table 4 The difference between potential evapotranspiration (Trabert, Rn-based, B-C, H-S) and real evapotranspiration (SEBS and SEBAL) in summer

Methods	July	SEBS	August	SEBS	September	SEBS	July-SEBS	August-SEBS	September-SEBS
H-S	256.3	243.2	231.8	237.4	196.6	165.8	0.1	0.0	0.2
B-C	212.5	243.2	199.5	237.4	171.4	165.8	0.1	0.2	0.0
Rn-based	131.8	243.2	124.3	237.4	114.7	165.8	0.8	0.9	0.4
Trabert	210.3	243.2	191.3	237.4	164.4	165.8	0.2	0.2	0.0

Methods	July	SEBAL	August	SEBAL	September	SEBAL	July-SEBAL	August-SEBAL	September-SEBAL
H-S	256.3	231	231.8	220	196.6	199	0.10	0.05	0.01
B-C	212.5	231	199.5	220	171.4	199	0.09	0.10	0.16
Rn-based	131.8	231	124.3	220	114.7	199	0.75	0.77	0.73
Trabert	210.3	231	191.3	220	164.4	199	0.10	0.15	0.21

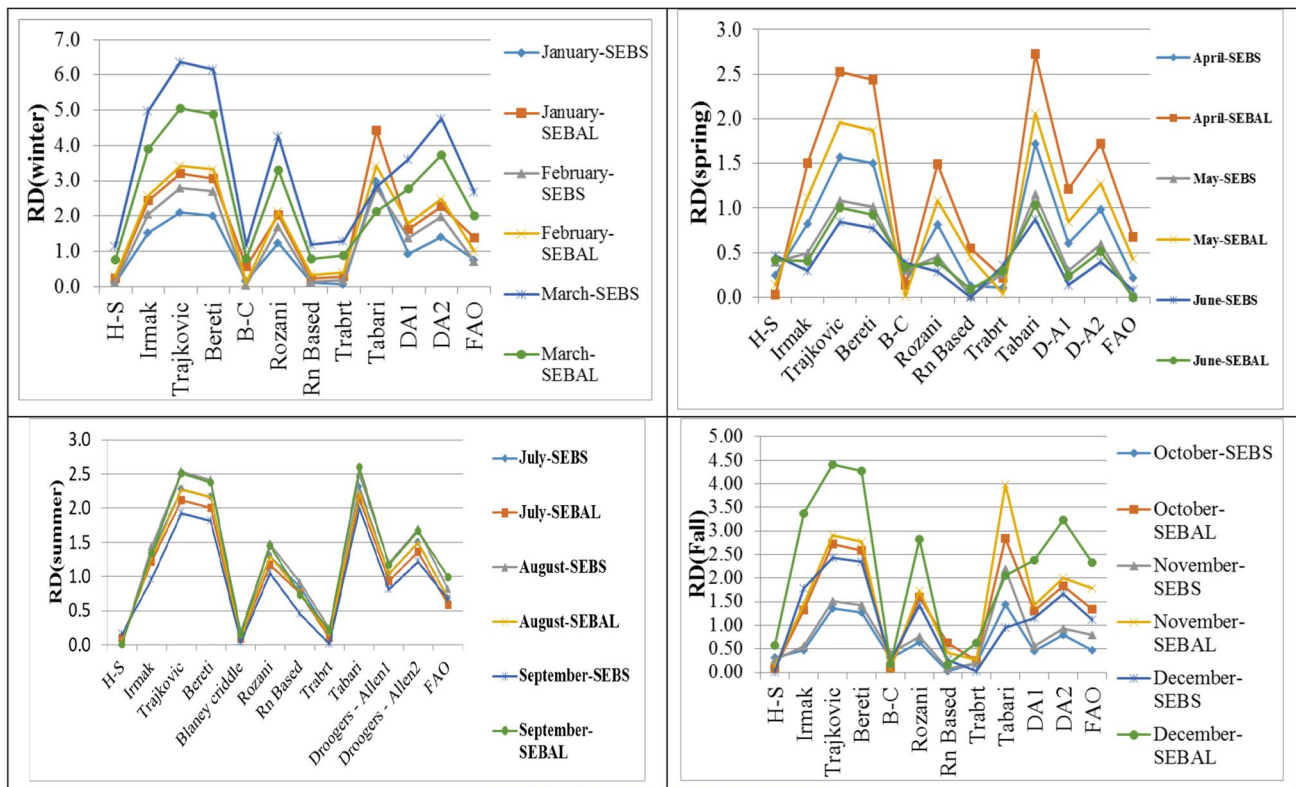


Fig. 9 Calculated error rate (RD)

Droogers–Allen1, Droogers–Allen2, and Rozani methods models were identified as the unsuitable methods with large RMSE (Fig. 10).

The final result of this section after comparing 12 experimental methods with the help of AD, RD, RMSE, showed that four methods (HS, BC, Trabert, Rn-based)

were identified as the best methods as the data are reliable and close to the results obtained from SEBS and SEBAL methods.

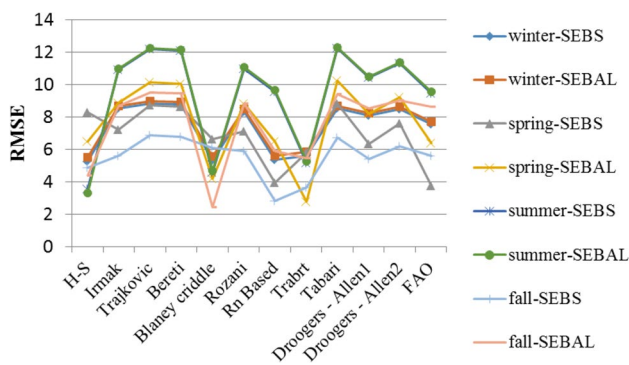


Fig. 10 Calculated error rate (RMSE)

4.7 Results of Water Requirement of SEBAL Algorithm and Experimental Methods

Kc values for pistachio 12 months in 2018–2019 based on monthly ET from SEBAL and ET0 from different empirical models are shown in Fig. 11. The H-S models worked well in estimating the crop coefficient (Kc) for pistachio crops during the summer and spring seasons (Fig. 11), as estimated Kc are within 0.5 and 1.5. H-S method has shown the water requirement of pistachios better than other methods. For example, Kc values (H–S) was in the summer, (0.9

and 1.1) and spring was (0.5 and 1), respectively. Kc values (H–S) in the autumn (0.6 and 1) were low due to reduced growth of plants in these seasons but winter (0.9 and 1.4) in winter the Kc was higher than in other months and this may be incorrect values.

Among other models, the Blaney-Criddle model yielded the closest Kc values, except for the 3 months of winter, when the estimated Kc values are 1.10 for the pistachio trees. Kc values (B-C) were (1.1 and 1.16) in summer, and (0.6 and 1.1) in spring, respectively. Kc values (Rn-based) were (1.73 and 1.8) in summer, and (1 and 1.5) in spring, respectively. The Trabrt model Kc values were (1.1 and 1.2) in summer, and (0.7 and 1.2) in spring respectively. While several models showed potential to produce reasonable Kc values for summer and spring, all of them showed a strong tendency to overestimate Kc values for winter (especially in March). However, H–S Blaney-Criddle, Trabert and Rn showed good potential for early and late seasons (Fig. 11).

4.8 Results of Water Requirement of SEBS Algorithm and Experimental Methods

Figure 12 shows Kc values for pistachio in all the 12 months in 2018–2019 based on monthly ET from SEBS and ET0 from different empirical models. Early and late season Kc for pistachio

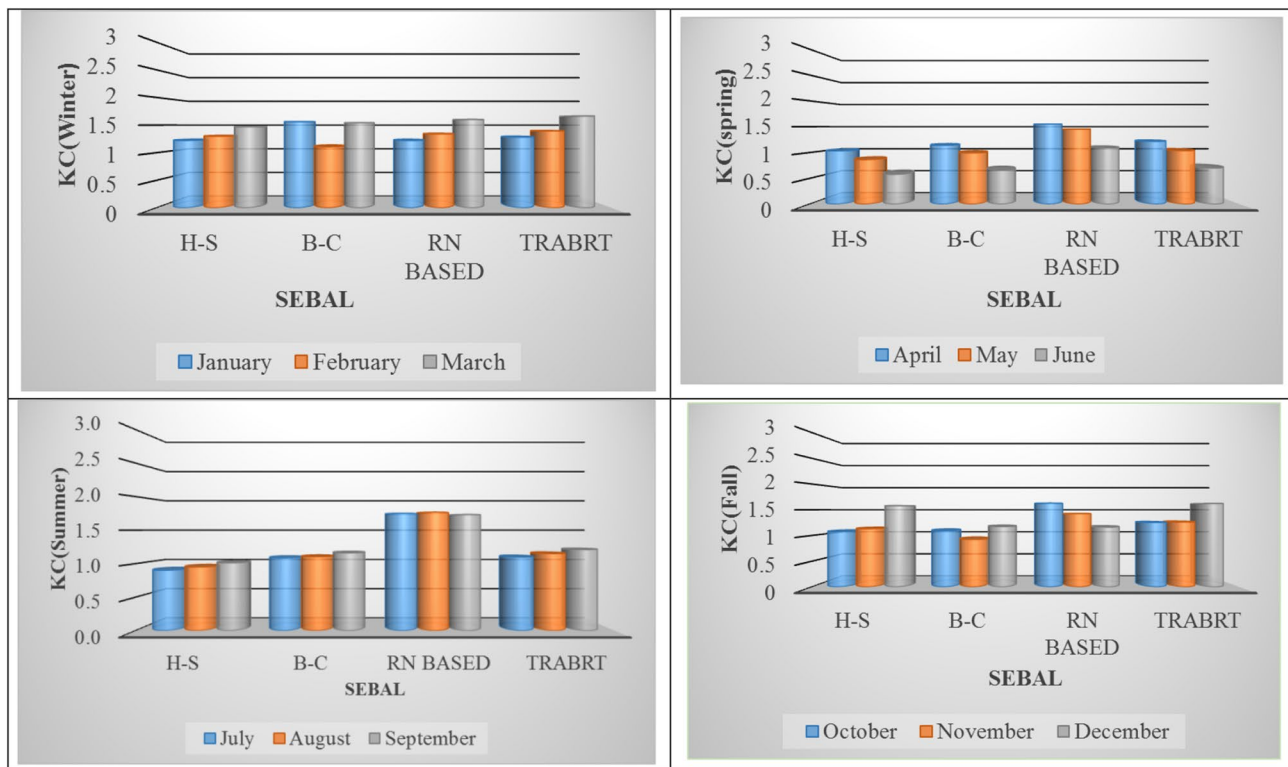


Fig. 11 Water requirement calculated using the SEBAL method and experimental methods

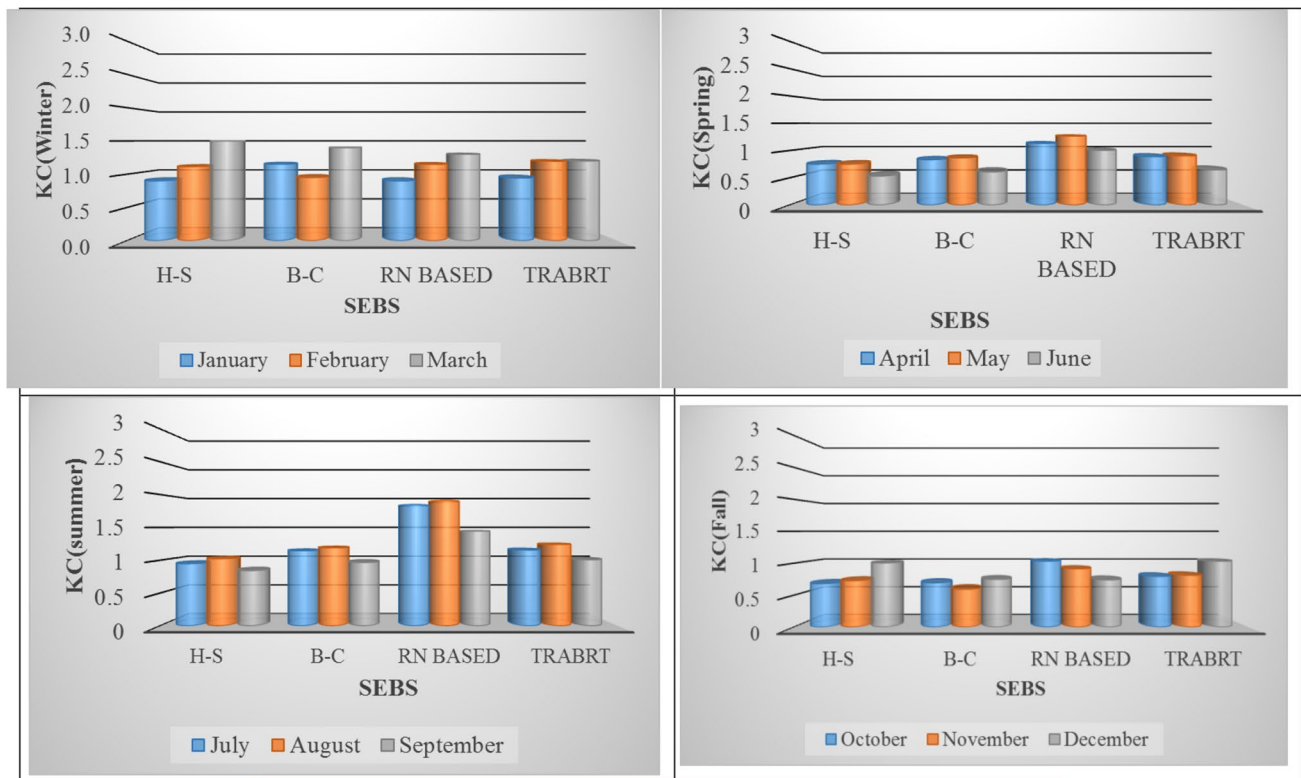


Fig. 12 Water requirement calculated by SEBS and experimental methods

crops is estimated by the H–S models (Fig. 12), in which the estimated Kc is shown to be within 0.9 and 1.9. Totally, H–S method was found to be the best-yielding Kc values for pistachios that were similar in most cases, as compared to the other empirical methods. For example, Kc values (H–S) in summer and spring were estimated as (0.9 and 1.1) and (0.5 and 0.7), respectively. Kc values (H–S) in autumn were low (0.6 and 1) due to the reduced growth of plants in these seasons but in winter Kc was higher (0.9 and 1.5) than that of other months and this may be because of unrealistic values like SEBAL model.

The closest Kc values were yielded by the Blaney-Criddle and Trabrt models, among other models, except for winter, when the estimated Kc values are 1.5 for the pistachio trees. Kc values (B-C) was (0.9 and 1.14) in summer and (0.6 and 0.8) in spring, respectively. Kc values based on the Trabrt model were (1.1 and 1.15) in summer and (0.6 and 0.9) in spring, respectively. Kc values (Rn-based) was (1.4 and 1.9) in summer and (1 and 1.2) in spring, respectively. While several models showed potential to offer realistic Kc values for summer and spring, all of them showed a strong tendency to overestimate Kc values for winter (especially in March). However, H–S Blaney-Criddle, Trabert, and Rn

models showed good potential for spring and summer seasons (Fig. 12).

5 Conclusions

Iran's climate is mostly arid and semi-arid and due to drought and poor management of water resources, this country has faced water shortage. The country, where groundwater is the primary source of water, has a long history of inefficiency in its water distribution network, particularly in the agricultural sector. While Iran may not currently experience food insecurity, the country encounters significant challenges in ensuring long-term access to water during periods of drought. One of the main pillars to calculate evapotranspiration is in arid and semi-arid regions like Iran. In this paper, we used the SEBAL and SEBS algorithms to estimate monthly ET for the 12 months in 2018–2019 via applying land sat satellite images across the plains of Dehshir in the central basin of Iran. Monthly actual evapotranspiration (ET) exhibited an increase from spring to summer, attributable to higher temperatures, irrigation practices, and enhanced vegetation

growth in pistachio orchards and agricultural lands. Based on the four methods of H-S, Blaney-Criddle, Rn and Trabert, the highest Kc is estimated in August and July and the lowest Kc is estimated in January. Results recommend that H-S, Blaney-Criddle, Rn,- and Trabert-based models can yield comparable ETO and Kc values to estimate the pistachio water requirements during early and late growing seasons. Other experimental methods, such as Trajkovic, Bereti, Tabari, Droogers–Allen1, Droogers–Allen2, and Rozani models were considered to be the unsuitable methods with large AD, RD, and RMSE. The required amount of water for pistachio trees in winter shows very unrealistic values of Kc. Results propose that in the area under our study, Trabert, Rn-based, B-C, H-S models have better potential in terms of estimating the pistachio water requirements, especially in summer and spring seasons.

Acknowledgements We appreciate the Iran Presidential Support Fund for supporting this research (No.: 97018501).

Declarations

Conflict of interest This manuscript has been read and approved by all the authors. The criteria for authorship have been met. The authors also do not have any financial interest or any other conflicts of interest.

References

- Abdullah KB (2006) Use of water and land for food security and environmental sustainability. *Irrig Drain J ICID* 55(3):219–222
- Allen RG, Tasumi M, Trezza R (2007) Satellite-based energy balance for mapping evapotranspiration with internalized calibration (METRIC)—model. *J Irrig Drain Eng* 133(4):380. [https://doi.org/10.1061/\(ASCE\)0733-9437](https://doi.org/10.1061/(ASCE)0733-9437)
- Allen RG, Pereira LS, Raes D, Smith M (1998) Crop Evapotranspiration Guidelines for computing crop water requirements. *FAO Irrig Drain Paper* 56(1):1–300
- Allen R, Tasumi M, Trezza R, Waters R, Bastiaanssen W (2002) SEBAL (Surface energy balance algorithms for land). *Adv. Training Users Manual*
- Bastiaanssen WGM, Menenti M, Feddes RA, Holtslang AA (1998) A remote sensing surface energy balance algorithm for land (SEBAL) formulation. *J Hydrol* 1(1):212–213
- Bastiaanssen WGM, Pelgrum H, Droogers P, Bruin HAR, Menenti M (1997) Area-average estimates of evaporation, wetness 3 indicators and top soil moisture during two golden days in EFEDA. *Agr and Forest* 87(4):119–137
- Bastiaanssen W, Chandrapala L (2003) Water balance variability across Sri Lanka for assessing agricultural and environmental water use. *Agric Water Manage* 58(1):171–192
- Bastiaanssen WG M (1995) Regionalization of surface flux densities and moisture indicators in composite terrain: a remote sensing approach under clear skies in Mediterranean climate. PhD Thesis, Wageningen University, Netherlands
- Brutsaert W (1982) Evaporation into the atmosphere: theory, history, and applications. D Reidel Publishing Company, Dordrecht
- Cosh MH, Stedinger JR, Ou SC, Liou KN, Brutsaert W (2007) Evolution of the variability of surface temperature and vegetation density in the Great Plains. *Adv Water Resour* 30(1):1094–1104
- Dinesh KG, Purushothaman BM, Vinaya MS, Suresh Babu S (2014) Estimation of evapotranspiration using MODIS sensor data in Udupi District of Karnataka, India. *Int J Adv Remote Sens GIS* 3(1):532–543
- Dube T, Shekede MD, Massari C (2023) Remote sensing for water resources and environmental management. *Remote Sens* 15(18):375–394
- Ehlers E, Krafft T (1996) German global change research. *Natl Comm Global Change Res Bonn* 1(1):1–128
- Elhag M, Psilovikos A, Manakos I, Perakis K (2011) Application of the SEBS water balance model in estimating daily evapotranspiration and evaporative fraction from remote sensing data over the Nile Delta. *Water Resour Manage* 25(1):2731–2742. <https://doi.org/10.1007/s11269-011-9835-9>
- Elhag M (2016) Inconsistencies of SEBS model output based on the model inputs: global sensitivity contemplations. *J Indian Soc Remote Sens* 44(3):435–442. <https://doi.org/10.1007/s12524-015-0502-0>
- Fabriki-Ourang S, MehrabadPurbenab S (2018) Evaluation of variations in physiological and biochemical traits in ancestral and evolutionary species of wheat under water deficit stress. *Environ Stresses Crop Sci* 11(4):791–802
- Fattahi M, Mehrshahi D (2018) Geomorphology and dating of the sand ramp (Kouh Rig) in Farashah, Taft, on the purpose of determining the last quaternary features of the northern slopes of Shirkouh. *J Geogr Res Desert Areas* 6(2):91–117. <https://doi.org/10.29252/GRD.2018.1239>
- Ferreira E, Mannaerts CM, Dantas AA, Maathuis BHM (2016) Surface Energy Balance System (SEBS) and satellite data For monitoring water consumption of irrigated sugarcane. *J Braz Assoc Agric Eng* 36(6):1176–1185. <https://doi.org/10.1590/1809-4430>
- Franklin PR, Gardner B, Mitchell RL (2010) *Physiology of crop plants*. Scientific Press
- Gao X, Miao S, Luan Q, Zhao X, Wang J, He G, Zhao Y (2019) The spatial and temporal evolution of the actual evapotranspiration based on the remote sensing method in the Loess Plateau. *Science Total Environ* 1(1):1–38
- Gao Y, Long D, Li Z (2008) Estimation of daily evapotranspiration from remotely sensed data under complex terrain over the upper Chao river basin in north China. *Int J Remote Sens* 11(1):3295–3315. <https://doi.org/10.1080/01431160701469073>
- Gibson LA, Munch Z, Engelbrecht J (2014) Particular uncertainties encountered in using a pre-packaged SEBS model to derive evapotranspiration in a heterogeneous study area in South Africa. *Hydrol Earth Syst Sci Kattenburg Lindau* 15:295–310
- Hyndman RJ, Koehler AB (2006) Another look at measures of forecast accuracy. *Int J Forecast* 22(4):679–688. <https://doi.org/10.1016/j.ijforecast.2006.03.001>
- Jafari M (2008) Revival of arid and desert areas. Tehran University Press, Tehran
- Kadam SA, Gorantwar SD, Das SN, Joshi AK (2014) Estimation of actual evapotranspiration by remote sensing. *Int J Innov Res Sci Eng Technol* 2(4):27–37
- Karimi M (2017) Irrigation planning in vineyards. Publication of agricultural education
- Kerr YH, Lagouarde JP, Nerry F, Ottlé C (2004) Land surface temperature retrieval techniques and applications: case of the AVHRR in thermal remote sensing in land surface processes. *Remote Sens Environ* 85(1):33–109. <https://doi.org/10.1201/9780203502174-c3>
- Kim N, Kim K, Lee S, Cho J, Lee Y (2020) Retrieval of daily reference evapotranspiration for croplands in South Korea using machine learning with satellite images and numerical weather prediction data. *Remote Sens* 12(1):3642

- Lillesand TM, Keifer W (1994) Remote sensing and image interpretation. Wiley 2(1):11–20
- Losgedaragh SZ, Rahimzadegan M (2018) Evaluation of SEBS, SEBAL, and METRIC models in estimation of the evaporation from the freshwater lakes (Case study: Amirkabir Dam, Iran). *J Hydrol* 561(1):523–531. <https://doi.org/10.1016/j.jhydrol.2018.04.025>
- Matin MA, Bourque CP (2013) Assessing spatiotemporal variation in actual evapotranspiration for semi-arid watersheds in northwest China: evaluation of two complementary-based methods. *J Hydrol* 486(1):455–465. <https://doi.org/10.1016/j.jhydrol.2013.02.014>
- Menenti M, Choudhury BJ (1993) Parameterization of land surface evapotranspiration using a location dependent potential evapotranspiration and surface temperature range. *Exch Processes Land Sur Range Space Time Scales* 212:561–568. <https://doi.org/10.4236/acs.2013.31008>
- Miryaghoubzadeh M, Solaimani K, Habibnejad Roshan M, Shahedi-KAbbaspour K, Akhavan S (2014) Estimation and assessment of actual evapotranspiration using remote sensing data (Case Study: Tamar Basin, Golestan Province, IRAN). *Iran Irrig Water Eng* 4(15):89–102
- Morse A, Tasumi M, Allen R G, Kramber WJ (2000) Application of the SEBAL methodology for estimating consumptive use of water and stream flow depletion in the bear river basin of Idaho through Remote Sensing, in Idaho. Department of Water Resources–University of Idaho
- Naeini MR (2017) Familiarity with planting and harvesting pistachio orchards. Nasim Hayat Publishing, New Delhi
- Piri H, Taher M (2019) Evaluation of 24 models of reference plant evaporation and transpiration in different climates of Iran. *Iran J Eco Hydrol* 6(3):611–622
- Rahimzadegan M, AdelehalSadat J (2019) Estimating evapotranspiration of pistachio crop based on SEBAL algorithm using Landsat 8 satellite imagery. *Agric Water Manag* 217(1):383–390. <https://doi.org/10.1016/j.agwat.2019.03.018>
- Ranjbar A, Pirasteh Anousheh H (2015) glance to the salinity research in Iran with emphasis on improvement of field crops production. *Iran J Crop Sci* 17(2):165–176
- Rizvi SA, Latif S, Ahmad M (2012) Mapping spatial disparity of canal water distribution under irrigated cropping environment using satellite imageries. *Int J Environ Sci Technol* 9(1):441–452. <https://doi.org/10.1007/s13762-012-0059-1>
- Semmens KA, Anderson MC, Kustas WP, Gao F, Alfieri GJ, McKee L, Prueger JH, Hain CR, Cammalleri C, Yang Y, Xia T, Sanchez L, Mar Alsina M, Vélez M (2015) Monitoring daily evapotranspiration over two California vineyards using Landsat 8 in a multi-sensor data fusion approach. *Remote Sens Environ* 185(1):155–170. <https://doi.org/10.1016/j.rse.2015.10.025>
- Senay GB, Friedrichs M, Singh M, Velpuri NM (2015) Evaluating Landsat 8 evapotranspiration for water use mapping in the Colorado River Basin. *Remote Sens Environ* 12(1):171–185. <https://doi.org/10.1016/j.rse.2015.12.043>
- Shamloo N, Sattari MT, Apaydin H, Khalil Valizadeh K, Prasad R (2021) Evapotranspiration estimation using SEBAL algorithm integrated with remote sensing and experimental methods. *Int J Digital Earth* 14(11):1638–1658
- Sharifan H, Ghahreman B, Alizadeh A, Mir Latifi SM (2006) Comparison of the different methods of estimated reference evapotranspiration (compound and temperature) with standard method and analysis of aridity effects. *J Agric Sci Nat Resour* 13(1):19–30
- Silva B, Mercante E, Boas MAV, Wrublack SC, Oldoni LV (2018) Satellite-based ET estimation using Landsat 8 images and SEBAL model. *Ciência Agronômica* 49(2):221–227. <https://doi.org/10.5935/1806-6690.20180025>
- Spaeth SC, HcRandau TR, Sinclair Vendeland JS (1984) Stability of soybean harvest index. *Agron J* 79(1):482–486. <https://doi.org/10.2134/agronj1984.00021962007600030028x>
- Srivastava PK, Suman S, Pandey V, Gupta M, Gupta A, Gupta DK, Chaudhary SK, Singh U (2021) Concepts and methodologies for agricultural water management. In *Agricultural Water Management: theories and Practices*. Academic Press, London
- Su Z (2002) The Surface Energy Balance System (SEBS) for estimation of turbulent heat fluxes SEBS-the surface energy balance. *Hydrol Earth Syst Sci* 6(1):85–100
- Su H, Wood E F, Wojcik R, McCabe M (2006) Sensitivity analysis of regional scale evapotranspiration predictions to the forcing data. American Geophysical Union, Fall Meeting 2007. abstract #H31A-02
- Su Z, Schmugge T, Kustas WP, Massman WJ (2010) An evaluation of two models for estimation of the roughness height for heat transfer between the land surface and the atmosphere. *J Appl Meteorol* 40(11):1933–1951. [https://doi.org/10.1175/1520-0450\(2001\)040%3c1933:AEOTMF%3e2.0.CO;2](https://doi.org/10.1175/1520-0450(2001)040%3c1933:AEOTMF%3e2.0.CO;2)
- Sumner DM (2001) Evapotranspiration from a cypress and pine forest subjected to natural fires, Volusia County, Florida, 1998–1999. In *Water-Resources Investigations Report USGS: Reston, VA, USA, 4245*.
- Tabari H, Grismer ME, Trajkovic S (2011) Comparative analysis of 31 reference evapotranspiration methods under humid conditions. *Irrig Sci* 1(1):107–117. <https://doi.org/10.1007/s00271-011-0295-z>
- Temesgen E (2009) Estimation of evapotranspiration from satellite remote sensing and meteorological data over the Fogera Floodplain–Ethiopia. International Institute for Geo-information Science and Earth Observation (ITC). Enschede, The Netherlands, MSc. Thesis.
- Van der Tol C, Verhoef W, Timmermans J, Verhoef A, Su Z (2009) An integrated model of soil-canopy spectral radiances, photosynthesis, fluorescence, temperature and energy balance. *Biogeosciences* 6(12):3109–3129
- Waters R, Allen R, Tasumi M, Trezza R, Bastiaanssen W (2002) SEBAL, advanced training and users manual. Idaho Implementation 1(1):1–97
- Yang W, Shabanov N, Huang D, Wang W, Dickinson R, Nemani R, Knyazikhin Y, Myneni R (2006) Analysis of leaf area index products from combination of MODIS Terra and Aqua data. *Remote Sens Environ* 104(3):297–312. <https://doi.org/10.1016/j.rse.2006.04.016>
- YounesazadehJalili S (2013) The effect of land use on land surface temperature in the Netherlands. Lund University, Lund

Springer Nature or its licensor (e.g. a society or other partner) holds exclusive rights to this article under a publishing agreement with the author(s) or other rightsholder(s); author self-archiving of the accepted manuscript version of this article is solely governed by the terms of such publishing agreement and applicable law.